NANO LETTERS
Letter
Cite This: Nano Lett. 2020, 20, 224−233
pubs.acs.org/NanoLett

Fundamental Limits to the Electrochemical Impedance Stability of Dielectric Elastomers in Bioelectronics

Paul Le Floch,[†] Nicola Molinari,[†] Kewang Nan,[†] Shuwen Zhang,[†] Boris Kozinsky,[†] Zhigang Suo,[†,‡] and Jia Liu*[,†]

[†]John A. Paulson School of Engineering and Applied Sciences and [‡]Kavli Institute for Bionano Science and Technology, Harvard University, Cambridge, Massachusetts 02138, United States

Supporting Information

ABSTRACT: Incorporation of elastomers into bioelectronics that reduces the mechanical mismatch between electronics and biological systems could potentially improve the long-term electronics−tissue interface. However, the chronic stability of elastomers in physiological conditions has not been systematically studied. Here, using electrochemical impedance spectrum we find that the electrochemical impedance of dielectric elastomers degrades over time in physiological environments. Both experimental and computational results reveal that this phenomenon is due to the diffusion of ions from the physiological solution into elastomers over time. Their conductivity increases by 6 orders of magnitude up to 10^{-8} S/m. When the passivated conductors are also composed of intrinsically stretchable materials, higher leakage currents can be detected. Scaling analyses suggest fundamental limitations to the electrical performances of interconnects made of stretchable materials.

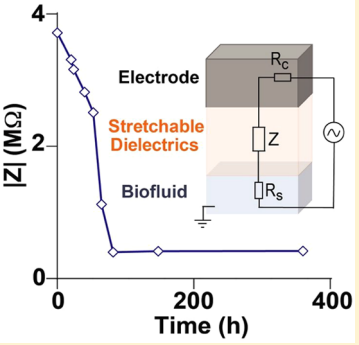

KEYWORDS: *Elastomer, stretchable bioelectronics, electrochemical impedance, ionic conductivity, bandwidth*

Reducing the mechanical mismatch between electronics and biological systems has been demonstrated as one of the important factors to enable chronically stable and minimally invasive bioelectronic interfaces for long-term, single-cell resolution, in vivo bioelectric interrogation and intervention, which are critical for biology and biomedicine.[1−4] Using stiff polymers to support and electrical passivation materials to encapsulate thin-film electronic components could realize flexible and stretchable bioelectronics.[5−10] In these cases, the flexibility of bioelectronics is quantified by their bending stiffness, which scales linearly with the elastic modulus of materials and the cube of the total thickness of devices. By reducing the thickness of devices, the bending stiffness becomes comparable to, or even smaller than, that of subcellular components, enabling tissue-level flexible bioelectronics, which have substantially improved the long-term stability and reduced the immunoresponse in soft tissue implantations (e.g., brain implants).[6−8,10] To prevent the electrical current leaking into the surrounding biofluid, the electrical passivation layer in this type of bioelectronics requires a thickness of hundreds of nanometers to micrometers. Further reducing the thickness of the devices has thus been limited by the dielectric performance of the passivation layer. Therefore, incorporation of low modulus and intrinsically stretchable materials such as elastomers and viscoelastic materials into bioelectronics that could reduce the effective bending stiffness as well as enable tissue-level soft, multilayer, and multifunctional bioelectronics has been actively pursued.[11−13] A variety of intrinsically stretchable material systems has been used in bioelectronics.[14,15]

However, the aforementioned bioelectronics require chronically stable device performance in which the electrical passivation layer should exhibit long-term stability in the physiological conditions comprising a warm ionic aqueous solution.[16,17] Results from our previous studies showed a coupling of stretchability and permeability in materials, suggesting that low-permeability and stretchability cannot coexist.[18] Above their glass transition temperature, elastomers are liquid-like at the molecular scale, which suggests that ion diffusion from biofluids in stretchable materials cannot be neglected over the typical lifetime of the device.

Here, we use the electrochemical impedance spectroscopy (EIS) to systematically characterize the electrochemical instability of elastomers used as dielectric passivation layers to encapsulate conductive interconnects in physiological conditions (e.g., 1× phosphate buffered saline (PBS)). The results show that the electrochemical impedance of dielectric elastomers decreases when they are exposed to physiological environments. This degradation occurs for all the tested elastomers with different moduli. Notably, impedance does not decrease when immersing elastomers in deionized (DI) water. The characteristic time of degradation follows a diffusion scaling when the thickness of the dielectric layer is changed. The conductivity of elastomers increases linearly with the surrounding ionic concentrations analogous to an aqueous electrolyte. When the interconnects are also composed of

Received: September 8, 2019
Revised: November 26, 2019
Published: November 28, 2019

DOI: 10.1021/acs.nanolett.9b03705
Nano Lett. 2020, 20, 224−233

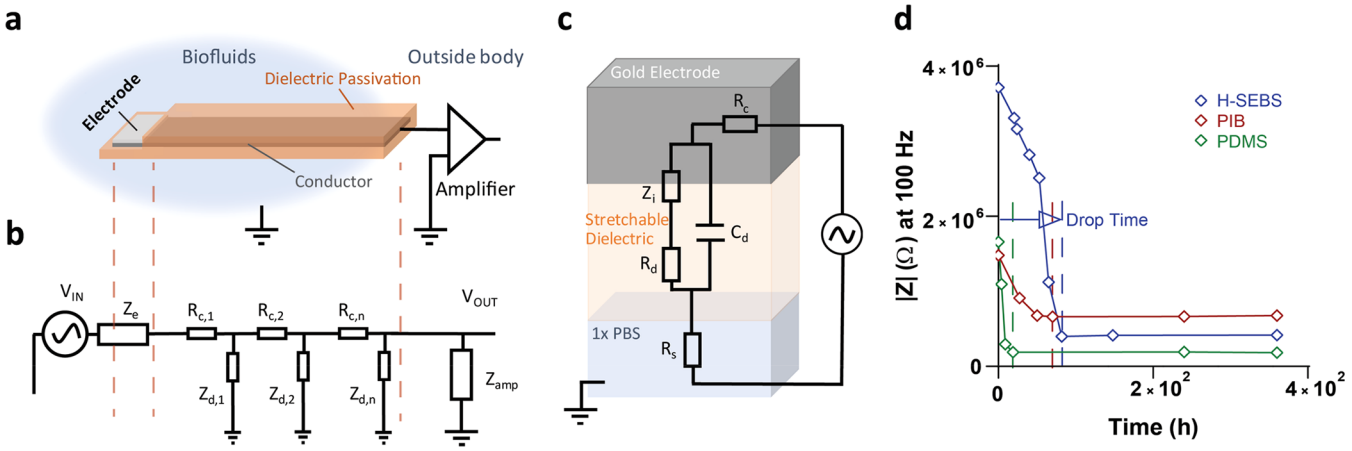

Figure 1. Dielectric performance degradation of elastomers in physiological solution. (a) Schematic shows the basic unit of bioelectronics that contains an electrode and a dielectric passivation layer encapsulated interconnect as a cable for signal collection and transmission to an external voltage amplifier. (b) Equivalent circuit diagram shows that the cable can be modeled as a conductive interconnect with the distributed resistance, R_c, insulated by the dielectric passivation layer with the distributed impedance, Z_d. V_{in}, Z_e, V_{out}, and Z_{amp} representing amplitude of the input signal, interfacial impedance of the electrode, amplitude of the output signal. and input impedance of the voltage amplifier, respectively. (c) Schematic shows the structure of the device used for the EIS characterization of elastomeric dielectric soaked in the physiological environment. The overlaid equivalent circuit diagram shows the components used to model the impedance collected from the EIS including series resistance in solution, R_s, and in conductor, R_c, interfacial impedance between the conductor and the dielectric, Z_i, bulk capacitance of the elastomer, C_d, and the resistance built by charged species in the elastomer, R_d. (d) Electrochemical impedance amplitude as a function of the soaking time in 1× PBS. Dashed lines separate the initial fast degradation and subsequent stability of the impedance after soaking. Arrow indicates how the drop time, t, is defined for a representative elastomer.

stretchable materials, we observed a further reduction of the electrochemical impedance. On the basis of the measured degradation, we predict the limitations to the dimensions and bandwidth of fully stretchable interconnects used in bioelectronics.

We are investigating the most basic component in bioelectronics, a passive voltage sensor,[19] which contains (i) an electrochemical impedance-based electrode for the signal collection, and (ii) a fully passivated conductor as the interconnect for the signal transmission from sensor to external amplifier and data acquisition system (Figure 1a). Both electrode and interconnect are immersed in biofluids. In conventional sensors made of stiff materials, the interfacial impedance of the electrode, Z_e, is smaller than the input impedance of the voltage amplifier, Z_{amp}. The series resistance of conductor, R_c, is negligible and the electrochemical impedance of the dielectric passivation, Z_d, is orders of magnitude larger than Z_e, R_c, and Z_{amp}. Collectively, they define the transmission efficiency of biological signals (i.e., a high V_{out}/V_{in} ratio, where V_{out} and V_{in} represent amplitudes of output and input signals, respectively). The bandwidth is further defined as the range of frequencies that can be transmitted along an interconnect above a certain level of attenuation (set by a given value of V_{out}/V_{in}). When the frequency of signals increases, Z_d decreases, which increases the signal attenuation. The bandwidth of an interconnect is usually estimated using a transmission line model,[20] accounting for the impedance of each component using lumped elements per unit length (Figure 1b).

To quantify the stability of the electrochemical impedance of dielectric elastomers, we use a three-electrode setup to measure the EIS of elastomer thin films soaked in aqueous solution over time[21] (Figures 1c and S1). Specifically, elastomers are spin-coated (thickness ∼3−25 μm) and cured on Cr/Au (5 nm/100 nm) thin-film electrodes of area 1 or 4 cm^2 (Figure S2). Samples are soaked in 1× PBS and DI water at 37 °C. After soaking, samples are washed by DI water quickly to remove the ionic residues on the surface of the sample and immersed in 1× PBS solution as the electrolyte for measurement. The thin-film gold electrode in each sample is used as the working electrode. A platinum wire (diameter 300 μm, 1.5 cm immersed) and a standard Ag/AgCl electrode are used as counter and reference electrodes, respectively. The distance between the counter and the working electrode is 1 cm. EIS is measured at a frequency range from 0.1 to 10^6 Hz. The overlaid equivalent circuits diagram shows the electrical model: a segment of dielectric elastomer is represented as a capacitor with bulk capacitance, C_d, which can be calculated using the intrinsic dielectric constant and thickness of the material. C_d is in parallel with a resistor, R_d, built by the charged species in elastomer, which we will calculate from the EIS characterization. We also consider the gold−elastomer interfacial impedance, Z_i, which is in series with R_d, given that the interfacial impedance comes from the metal−electrolyte double layer built by charged species diluted in the elastomer. The combination of R_d, C_d, and Z_i represents the dielectric impedance of the elastomer.

We investigated three commercially available dielectric elastomers that are used in stretchable bioelectronics: styrene−ethylene−butylene−styrene copolymer (SEBS), polyisobutylene (PIB), and polydimethylsiloxane (PDMS). Figure 1d summarizes the magnitudes of their representative impedances at 100 Hz as a function of the soaking time. Notably, we observe a significant reduction of all impedances to a lower equilibrium value after a characteristic drop time, t. This phenomenon is consistently observed among all three elastomers with various thicknesses (Figure 1d). Because the electrochemical interfacial impedance of a nonpassivated gold electrode in 1× PBS (Figure S3) is more than 3 orders of magnitude smaller than that of a passivated electrode, the reduction of impedances in passivated electrodes comes mostly from the reduction of impedances in elastomer dielectric

DOI: 10.1021/acs.nanolett.9b03705
Nano Lett. 2020, 20, 224−233

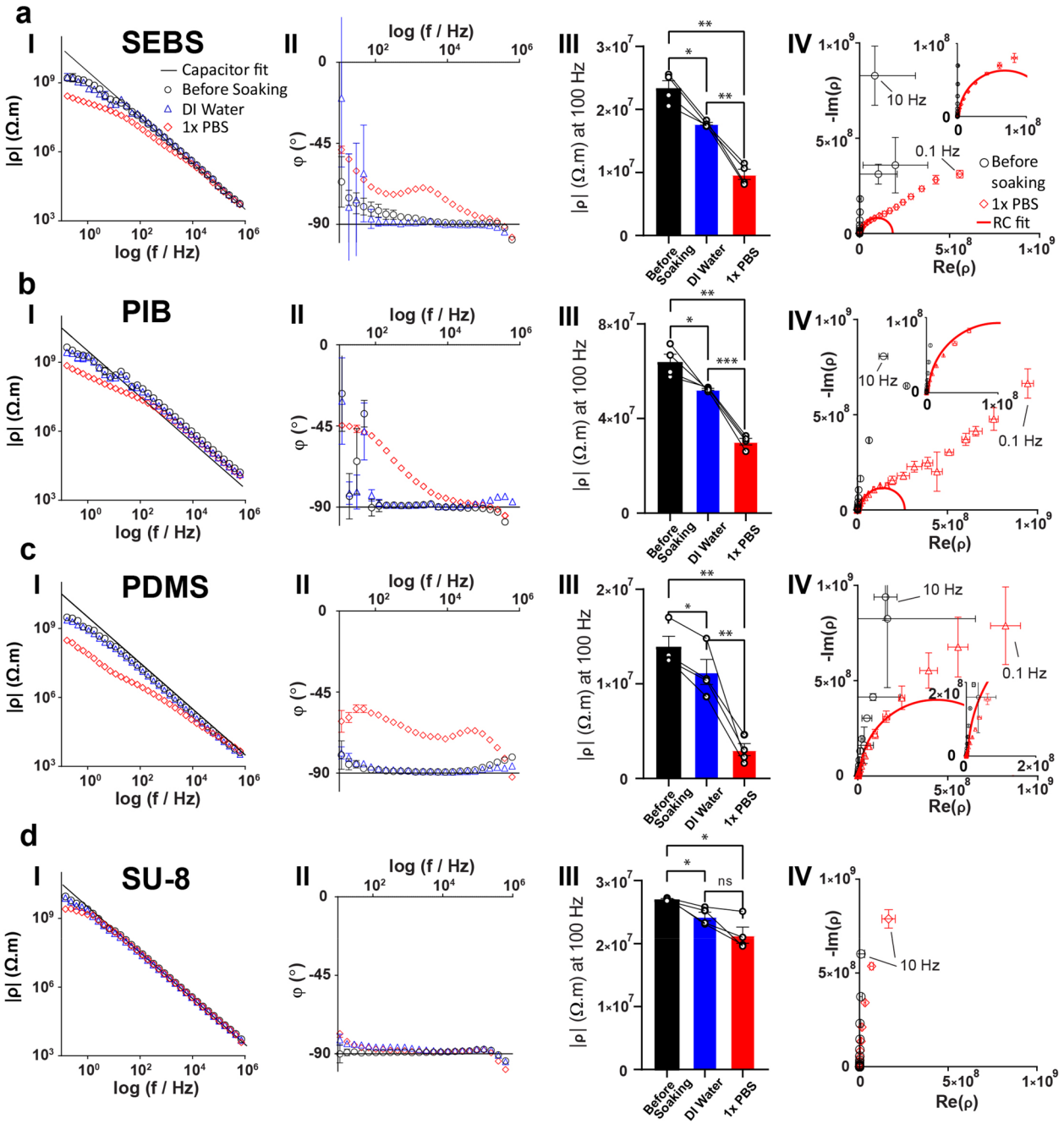

Figure 2. EIS characterization of dielectric polymer films in aqueous solutions. (a–d) EIS characterization of SEBS (a), PIB (b), PDMS (c), and SU-8 (d). (I, II) Bode plots of the normalized impedance of polymer films before soaking in aqueous solution after 1 week soaking in DI Water and subsequently after 1 week soaking in 1× PBS. All the soaking experiments are conducted at 37 °C. Capacitance fits in (I) are calculated based on the dielectric constant of each polymer from literature.[40] (III) Statistic summary of normalized impedance at 100 Hz before and after soaking in DI water and 1× PBS. Value represents mean ± S.D.; $n = 4$; *, $P < 0.05$; **, $P < 0.01$; ***, $P < 0.001$; paired, two-tailed t test. (IV) Nyquist plots of EIS characterization on polymer film before and after soaking in 1× PBS (value represents mean ± S.D.). The zoom-in panels show the high-frequency region of the plot.

layers. To eliminate the potential effect from water diffusion and polymer swelling, we measured the EIS from each sample before soaking, after 1-week soaking in DI water at 37 °C, and after another 1-week soaking in 1× PBS at 37 °C (Figure 2). In addition, we prepared a control sample using the epoxy-based, nonstretchable SU-8 2002 as a dielectric layer coated on the gold electrodes with the same geometry and soaked in the same aqueous solutions for EIS characterization. To compare values from different samples, we normalize the impedance by the ratio of the electrode's area to its thickness as complex resistivity, ρ. Results show that $|\rho|$ of all elastomers drops slightly after samples are immersed in DI water and drops significantly after they are immersed in 1× PBS (Figure 2b–c, I), whereas the $|\rho|$ of control samples remains similar (Figure 2d, I). Notably, for many elastomer samples even less than 1 week soaking in 1× PBS is sufficient to reduce the values of $|\rho|$ at 100 Hz to the equilibrium state. In addition, phase plots show the phase values of all elastomer samples increase

DOI: 10.1021/acs.nanolett.9b03705
Nano Lett. 2020, 20, 224–233

significantly toward less-negative values after soaking in 1× PBS (Figure 2b–c, II), whereas phase values of control samples remain at −90° (Figure 2d, II). Large standard deviations on the phase plots at low frequencies can be attributed to the limitations of the equipment, which we explain in Supporting Information. Statistical analysis shows that the values of $|\rho|$ at 100 Hz from all three elastomers drop significantly after soaking in 1× PBS compared to the value after soaking in DI water (Figure 2b–c, III), whereas the slight drop of impedances after DI water soaking of control samples is not significant (Figure 2d, III).

Nyquist plots of ρ (Figure 2b–c, IV) show similar shapes for all of three elastomers: from high to low frequencies, the plot is first curved toward higher resistances (horizontal axis) and then follow a line of constant slope. This trend is analogous to the Randles[21] cells model of electrolyte–metal interfaces, as the electrical model proposed in Figure 1c. At high frequencies, the metal–elastomer interfacial impedance is negligible because the electrical double layer impedance is small. Therefore, we can model the high-frequency regime (arbitrarily defined as frequencies above 10 Hz) of the Nyquist plot by a simple R_d–C_d parallel circuit (Figure S4). It corresponds to the curved part of the Nyquist plot. First, C_d is determined by the bulk, pristine capacitance of the dielectric elastomer before soaking in aqueous solutions. Second, we can determine R_d using the R_d–C_d model to fit the Nyquist plots after soaking. Details of the fitting procedure are described in Supporting Information. Similar Nyquist plots and electrical equivalent circuits have been used to model the EIS of single ion–polymer electrolytes.[22−25] Third, from the measured R_d we can extrapolate the ionic conductivity, σ_d using eq 1, where H_d is the thickness of the dielectric layer and A is area of the electrode. The thickness of each sample is in the range of 3–10 μm and measured by contact profiler (Figure S5)

$$\sigma_d = \frac{1}{R_d}\frac{H_d}{A} \tag{1}$$

We summarize σ_d for all of the investigated elastomers in Table 1. The values are in the range $9 \times 10^{-9} - 5 \times 10^{-8}$ S/m,

Table 1. Ionic Conductivities, Ions Diffusion Coefficient, and Molar Concentration of Ions Inside Elastomers

material	σ (S/m)[a]	D (m^2/s)[b]
SEBS	$(9.44 \pm 0.70) \times 10^{-9}$	$3.8 \times 10^{-17} < D < 7.5 \times 10^{-17}$
	$(5.18 \pm 2.87) \times 10^{-8}$[c]	
PIB	$(2.28 \pm 1.40) \times 10^{-8}$	$6.0 \times 10^{-17} < D < 8.0 \times 10^{-17}$
PDMS 10:1	$(4.45 \pm 2.68) \times 10^{-8}$	$9.0 \times 10^{-17} < D < 1.1 \times 10^{-16}$
	$(2.96 \pm 0.99) \times 10^{-8}$[d]	

[a]At 23 °C after aging in 1× PBS [b]At 37 °C. [c]AgNP electrode. [d]CNT electrode.

which can be compared to previously reported ionic conductivity of polyvinyl chloride films soaked in 0.2 mM potassium chloride solutions (2.5×10^{-12} S/m),[26] but are still orders of magnitude lower than single ion–polymer electrolyte conductivities.[22−24,27]

Several observations suggest that the conductivity is due to the diffusion of ions in the elastomers. First, the impedance does not degrade when samples are just immersed in DI water (Figure 2). Second, typical diffusion coefficients of water for elastomers fall in the range $10^{-9} - 10^{-11}$ m^2/s,[18,28,29] which suggests that the diffusion of water across a micrometer-thick elastomer reaches equilibrium within seconds. Third, when ions diffuse into an elastomer thin film, the drop time, t, of the electrochemical impedance should be related to the thickness of the film.[30] We plot the thickness, H, of various samples as a function of t in log scale (Figure 3a). For each elastomer, the trend closely follows the line with a slope of 0.5, which is characteristic of Fickian diffusion. We can extrapolate an effective diffusion coefficient, D, following the scaling relation[30]

$$H = \sqrt{Dt} \tag{2}$$

Resulting statistics of effective diffusion coefficients for all three dielectric elastomers are summarized in Table 1. Fourth, we measure the change in ionic conductivity of SEBS as a function of the surrounding PBS soaking concentration. The Nyquist plots for a given sample subsequently immersed in 1×, 2×, and 5× PBS (Figure 3b) show that the impedance real component has a higher value as the ionic concentration increases. Ionic conductivities are extrapolated from R_d–C_d fit and normalized to σ_0 (conductivity from samples just immersed in 1× PBS). Normalized ionic conductivity is plotted as a function of PBS concentration (Figure 3c), which shows that the ionic conductivity of the elastomer increases almost linearly with the increase of PBS concentration in this range, analogous to a dilute electrolyte.

Taylor et al.[26] also observed that the salt concentration of an electrolyte in contact with a polyvinylchloride film decreases quantitatively after reaching equilibrium, indicating that a substantial amount of ions can be absorbed by the polymer. It could be argued that the ionic conductivity of the elastomer is due to the presence of pores and pinholes filled with physiological solution in the film. In this case, $\sigma_d = 10^{-8}$ S/m would correspond to a fraction of the surface of about 5×10^{-9} covered by such defects. However, the diffusion rate should be similar to that of DI water through the bulk elastomer in that case.

To better understand this diffusion process, we performed molecular dynamics (MD) simulations to compare the diffusion of water and sodium chloride in stiff polymer versus elastomer (molecular structures between SU-8 versus PIB). Details on the simulation procedure are given in Supporting Information (Figures S6 and S7, Table S1). The mean square displacement (MSD) of the sodium ion inside the polymers is plotted as a function of simulation time for different temperatures (Figure 3d). The results show that the MSD of the sodium ion in PIB is 1 order of magnitude higher than that in SU-8 at 300 K. When the temperature is increased above the glass transition temperature of SU-8, the MSD between PIB and SU-8 becomes closer to each other. Extrapolated diffusion coefficients are shown in the Arrhenius plot (Figure 3e) for PIB. The diffusion coefficients of ions are >3 orders of magnitude smaller than that of water in the elastomer at ambient temperature. From the linear fitting of the Arrhenius plot, in PIB the diffusion coefficient of water is 2.1×10^{-11} m^2/s, whereas the average diffusion coefficient of sodium and chloride ions is 1.8×10^{-14} m^2/s. These simulation results explain some of our experimental results: (i) ions diffuse slower than water in elastomers. (ii) ion diffusion is much slower in PIB than in SU-8, especially at ambient temperature, which is below the glass transition temperature of SU-8. However, the simulated diffusion coefficient for PIB is 2 to 3 orders of magnitude larger that the effective ionic diffusivity we measure, which suggests a more complicated situation in ion diffusion, such as solvation of ions by water molecules, or ion–

DOI: 10.1021/acs.nanolett.9b03705
Nano Lett. 2020, 20, 224−233

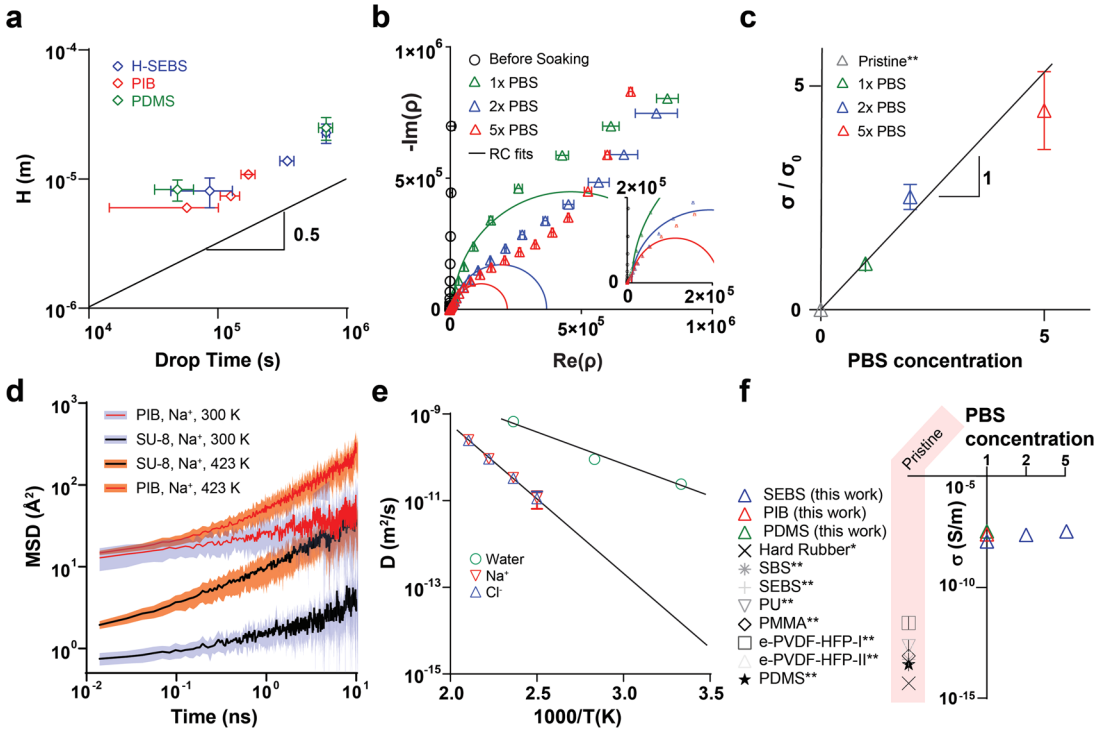

Figure 3. Characterization and modeling of ion diffusion in elastomers. (a) Thickness of elastomers as a function of the drop time defined in Figure 1d. (b) Nyquist plots of EIS characterizations for representative SEBS dielectrics with thickness of 3.6 ± 0.2 μm immersed in PBS with different ionic concentrations. Values represent the electrochemical impedance of the film after reaching the equilibrium state in different PBS solutions. The zoom-in panel shows the high frequency region of the plot. (c) Relative ionic conductivity to the concentration of PBS based on the semicircle fits for SEBS. Value represents mean ± SD. (d) Means square displacement (MSD) of sodium ions in SU-8 and PIB at temperatures below and above the glass transition temperature for SU-8 as a function of simulation time. (e) Extrapolated diffusion coefficient of water and ions in a computer-generated PIB structure to 1000/temperature based on five computer-generated structures for each data point. (f) Ionic conductivities of elastomers extrapolated using the electrical model of Figure 1c as a function of PBS concentration. **, Data points from the work of reference 31.

ion correlation, which might increase the effective size of the diffusants and slow down the diffusion.

When soaked in 1× PBS solution, the ionic conductivity of elastomers is in the range $\sigma = 10^{-8}$ S/m, which is 2−6 orders of magnitude higher than that of pristine elastomers (Figure 3f). Although the effective diffusion coefficients for all three dielectric elastomers are 10^{-17} to 10^{-16} m^2/s, which are smaller than typical diffusion coefficients of water in elastomers and plastics, we can estimate, using equation 2, that it requires at least 40 μm thick elastomeric passivation to prevent ion penetration to the electroactive layers in 1 year.[18,28,29] Notably, the bending stiffness of a 40 μm thick elastic passivation layer, however, is comparable to or even higher than that of a 1 μm thick SU-8 passivation layer. In this regard, for ion-sensitive devices using dielectric elastomers as electrical encapsulation cannot further reduce the bending stiffness compared to a device using stiff polymers.

In addition, in the real application the dielectric elastomer is used to insulate stretchable conductors. Because our data demonstrate that the degradation of the impedance is due to the diffusion of ions in stretchable materials, we hypothesize additional reasons that the degradation of the impedance could happen to the device in which both conductor and dielectrics are stretchable. First, the network or porous structures of the stretchable conductor have larger surface areas than metal conductors. Second, ions diffused across the dielectric elastomer can further diffuse into the stretchable conductor (Figure 4, I). To test our hypothesis, we fabricate two fully stretchable dielectrics-conductor systems: (i) printed commercial Ag nanoparticles (AgNP)−polymer composite (Figure 4a) with SEBS as the dielectric layer, and (ii) single-wall carbon nanotubes (Figure 4b) with PDMS as the dielectric layer (see Supporting Information, Methods). After fabrication, the integrity of both systems is checked by microscopic imaging (Figure S8). We characterize the chronic stabilities of parasitic electrochemical impedance and series resistance of the nonpassivated stretchable electrodes in 1× PBS. The results confirmed that both values, after samples are immersed in 1× PBS over the same period of time as previous testing, are still orders of magnitude lower than the impedance from dielectric elastomers (Figures S9 and S10). After 1 week immersion in 1× PBS, the EIS characterizations on SEBS/AgNP and PDMS/CNT systems show that $|\rho|$ values of fully passivated electrodes drop significantly (Figure 4, II) and the phase values increase toward less negative values (Figure 4, III). Notably, the change in $|\rho|$ from the passivated stretchable electrodes is much higher than that from the passivated gold electrodes at low frequencies. Statistical results (Figure 4, IV) confirm statistically significant drops at 100 Hz. The R_d−C_d semicircles that fit the low frequency regime from Nyquist plots (Figure 4, V) show that the ionic conductivities of SEBS/AgNP and PDMS/CNT are comparable to these from SEBS/gold and PDMS/gold electrodes (Table 1), which further confirms that ionic diffusion is an intrinsic property for dielectric elastomers. The above results suggest that intrinsically stretchable interconnects have a higher low-frequency electrical loss compared to nonstretchable interconnects due to the ionic

DOI: 10.1021/acs.nanolett.9b03705
Nano Lett. 2020, 20, 224−233

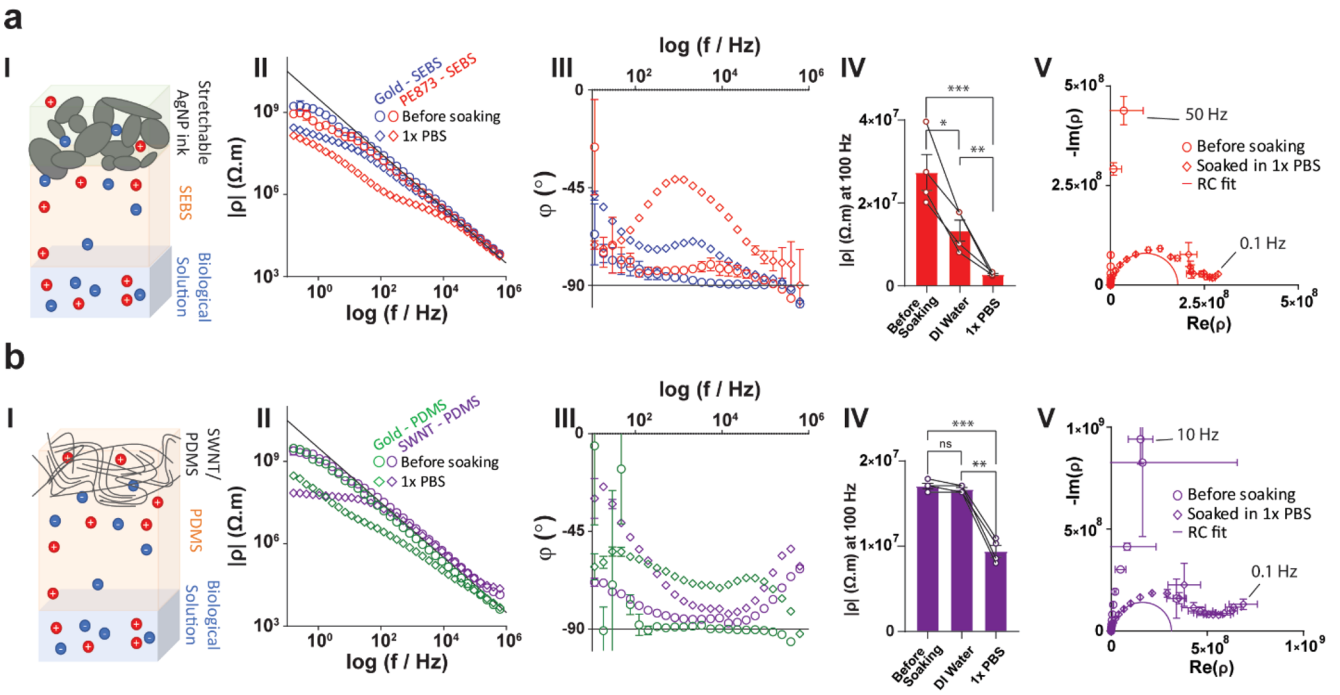

Figure 4. EIS characterization of intrinsically stretchable electrode−elastomeric passivation devices. (a,b) Schematics and EIS characterization of representative fully stretchable devices: SEBS/stretchable Ag nanoparticles (AgNP, PE873) conductor (a) and PDMS/CNT conductor (b) before and after soaking in 1× PBS. (I) Schematics show fully stretchable device structures for EIS characterization. (II, III) Normalized impedance bode plots (II) and phase plots (III) of EIS compare the gold electrode−elastomer device and the intrinsically stretchable electrode−elastomer device before and after reaching the equilibrium state when soaking in 1× PBS. All the soaking experiments are conducted at 37 °C. Capacitance fits in (II) are calculated based on the dielectric constant of each polymer. (IV) Statistic summary of normalized impedance at 100 Hz of fully stretchable devices before and after soaking in DI water and 1× PBS for 1 week. Value represents mean ± S.D.; $n = 4$; *, $P < 0.05$; **, $P < 0.01$; ***, $P < 0.001$; paired, two-tailed t test. (V) Nyquist plots of EIS characterization on fully stretchable devices before and after 1 week soaking in 1× PBS. Value represents mean ± SD.

conductivity from dielectric elastomers and high parasitic capacitance from the stretchable conductor.

We envision that this electrical loss will reduce the bandwidth of the signal transmission. In our empirical model (Figure 1c), the dielectric's electrical properties are described by two parameters: its bulk capacitance with a dielectric constant, ε_d, and its ionic conductivity, σ_d. Then, a cutoff frequency, f_d, can be defined by eq 3

$$f_d = \frac{1}{2\pi}\frac{\sigma_d}{\varepsilon_d} \tag{3}$$

When the frequency of signals is larger than f_d, the elastomer behaves as a capacitor, in which the bulk capacitance will dominate its impedance. When the frequency of signals is smaller than f_d, the elastomer behaves as a conductor in which impedance shows more resistive characteristics. Bandwidth for bioelectrical signal transmission is typically from 1 Hz to 10 kHz. When the conductivity of the dielectric passivation layer increases, f_d can reach to this range of frequency causing a higher leakage current from the ionic conduction and thus reducing the bandwidth of the interconnect. For a pristine elastomer, Kong et al.[31] report a conductivity $\sigma_d \cong 10^{-13}$ S/m. However, the typical ionic conductivity measured for these three elastomers that we measured (Table 1) has $\sigma_d \cong 10^{-8}$ S/m after soaking in 1× PBS solution. When we choose the relative permittivity of the elastomer, $\varepsilon_r = 3$, we can calculate the $\varepsilon_d \cong 2.7 \times 10^{-11}$ F/m through $\varepsilon_d = \varepsilon_r\varepsilon_0$. Thus, the cutoff frequency is $f_d \cong 5.9 \times 10^{-4}$ Hz for a pristine elastomer and $f_d \cong 5.9 \times 10^{1}$ Hz for an elastomer soaked in PBS solution. The natural frequency is shifted within the frequency range of interest, which can decrease the bandwidth of devices when elastomers are used as electrical passivation.

The importance of ionic leakage currents depends on the geometry of the interconnects. To test the transmission losses through the stretchable interconnects, we test 40 cm long, 14 μm-thick, and 200 μm-wide SEBS/AgNW interconnects with 4 μm-thick SEBS layer (Figure 5a,b and Figure S8). We soak the device in PBS solution at 37 °C and characterize the bandwidth of the interconnect over time using the rising time method (Figure 5c). Specifically, a voltage pulse is sent at one end of the interconnect and measured at the other end using a voltage digitizer (Axon Digidata 1550B). The interconnect is surrounded by grounded 1× PBS solution. The empirical relation between rise time T and bandwidth, defined as the frequency with 3 dB losses for single pole filter roll-off in the frequency domain, is

$$\text{Bandwidth (Hz)} = \frac{0.35}{T(s)} \tag{4}$$

The results show that the bandwidth of the device soaked in PBS decreases over time (Figure 5d), whereas the sample immersed in DI water does not degrade after 1 week soaking. We need to acknowledge that even a lossless dielectric will have a finite bandwidth. Therefore, the transmission line model is used to determine the bandwidth of a conductive interconnect.[20] A similar model can be used to predict the effect of ionic conductivity on the bandwidth of an interconnect insulated by a dielectric elastomer (Figure 5e).

DOI: 10.1021/acs.nanolett.9b03705
Nano Lett. 2020, 20, 224−233

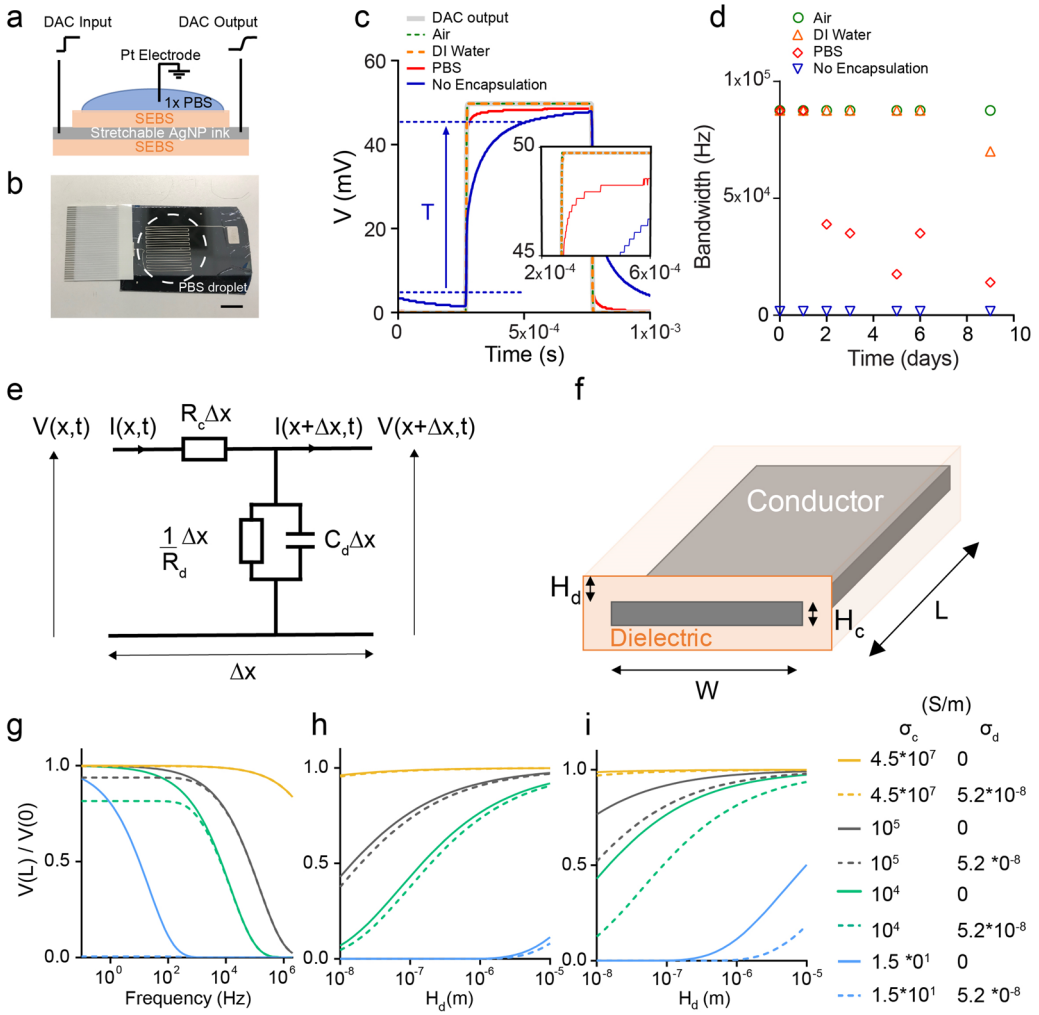

Figure 5. Measurement and simulation of bandwidth in fully stretchable interconnects. (a) Schematic shows a fully stretchable interconnect setup for the bandwidth measurement. (b) Photography of the setup. The conductive line is 40 cm long, 14 μm thick, and 200 μm wide. The encapsulation is about 4 μm thick ($2L^2/(H_c{*}H_d) = 5.8 \times 10^9$). The surrounding solution is grounded by the platinum electrode. A pulse signal (50 mV, 1 ms duration) is sent through the stretchable conductor and recorded by the data acquisition card (DAC). (c) Signals that are transmitted through the fully stretchable interconnect are recorded by DAC through the setup in (a) at different conditions. The rise time, T, of the signal is measured for calculation of bandwidth. The zoom-in panel highlights the difference in rise time between various samples. (d) Bandwidth as a function of soaking time calculated from measurements. (e) Equivalent circuit diagram shows the simplified electrical model (assuming interfacial impedance is significantly smaller than the ionic conductance of the dielectric elastomer) of the fully stretchable interconnect. (f) Schematic shows the structure of a fully stretchable interconnect and its geometric factors for scaling analysis. (g) Relative amplitude attenuation of signals propagated along different interconnects for a geometrical factor $2L^2/(H_c{*}H_d) = 8 \times 10^9$. (h,i) Relative amplitude attenuation of signals as a function of the thickness of dielectric H_d at 1 kHz (h) and 100 Hz (i), all the other parameters for simulation are the same as (g).

In this case, we neglect the interfacial impedance of the conductor for simplicity. Because the attenuation of the signal at low-frequencies depends on the geometry of the electrode and the properties of the conductor, we derive the formula for the amplitude of a forward-traveling voltage wave going along the interconnect as a function of material parameters and geometry for a stripline interconnect (Figure 5f, Supporting Information)

$$\left|\frac{V(L)}{V(0)}\right| = \left|\exp\left(-\sqrt{\frac{1}{f_c}(jf + f_d)}\right)\right| \tag{5}$$

with $f_c = \frac{1}{4\pi}\frac{H_c H_d}{L^2}\frac{\sigma_c}{\varepsilon_d}$ and, f as the frequency of the forward-traveling wave. In eq 5, f_c is directly related to the bandwidth upper band for a lossless transmission line. Low-frequency losses depend on the ratio f_d/f_c, which can be expressed as

$$\frac{f_d}{f_c} = \frac{2L^2}{H_c H_d}\frac{\sigma_d}{\sigma_c} \tag{6}$$

It is noteworthy that eq 6 is independent of the size scale of the interconnect. However, the diffusion time for ions will increase as the square of the thickness of dielectric, H_d. From eq 2 and the values of ionic diffusivities measured (Table 1), we estimated that a device insulated by a 40 μm think dielectric elastomer could be sustained for one year. Considering a typical dimension of a bioelectronic interconnect where width W = 10 μm, thickness of conductor H_c = 100 nm, thickness of dielectric H_d = 1 μm, and length L = 2 cm, we plot the relative voltage amplitude of a forward-wave that propagates along the stripline interconnect as a function of

DOI: 10.1021/acs.nanolett.9b03705
Nano Lett. 2020, 20, 224−233

frequency for different values of conductivity of the conductor (from 1.5×10^1 to 4.5×10^7 S/m) and the dielectric (either 0 or 5.18×10^{-8} S/m), respectively (Figure 5g). This model does not consider the electrode−dielectric elastomer interfacial impedance. However, for the aforementioned geometry of the device and σ_d of the dielectric elastomer, which represents standard values for many stretchable devices,[32−39] there is a significant low-frequency loss when $f_d \ll f_c$ ($\sigma_c \ll 4 \times 10^2$ S/m). Notably, when gold electrodes are used as conductors due to their high σ_c (4.5×10^7 S/m) the ionic leakage current through the elastomer is negligible. These results suggest that the low-frequency losses through the dielectric elastomer are imperceptible for the same geometric interconnects comprised of highly conductive materials. In contrast, when the same interconnects are comprised of materials with low conductivity (e.g., hydrogel and ionic liquid conductors), low-frequency losses will become significant when the electrode is immersed in biofluids over time. Lastly, for the standard stretchable conductors based on CNT electrodes and silver-nanoparticle polymer composites, although their initial conductivities can reach 10^5 S/m,[14,38] the conductivities decrease after a few cycles of mechanical stretching[39] so that low-frequency losses can still become significant in this type of electrode over time.

In addition, to make this discovery tangible to the real application, we calculate the signal attenuation to the thickness of elastomer passivation layer. Notably, the lossy transmission line model can also predict the level of leakage current. When a monochromatic forward-traveling wave reaches the amplifier (Figure 1a), voltage and current attenuation, defined as $\left|\frac{I_{OUT}}{I_{IN}}\right|$, follow the same scaling (eq 6). Figure 5h,i show the calculated attenuation of signal at 1 kHz and 100 Hz, respectively, transmitted along interconnects with thickness of dielectric layer from 10 nm to 10 μm. The result first suggests that when the thickness of the elastomer encapsulation is reduced, the relative amplitude of signals will be further reduced due to the ionic leakage current through the dielectric elastomer encapsulation (Figure 5h). Importantly, this reduction will be significant at a frequency of 100 Hz and below (Figure 5i). Notably, besides the thickness of the dielectric layer, the length of interconnect will affect even more the signal attenuation (eqs 5 and 6) because f_c scales as $1/L^2$. Second, for conductors with conductivity that is higher than 10^4 S/m, even a 200 nm thick dielectric elastomer encapsulation can allow >50% signal at 1 kHz or beyond to be transmitted, which is a typical value for the best state-of-the-art stretchable conductors.[36,39] However, we need to recognize that other factors may become important at the nanoscale, such as chronic chemical stability of elastomers, crosstalk between neighboring electrodes for multielectrode arrays, and mechanical stability of soft, multimaterial composite structure.

In conclusion, we have investigated the chronic stability of electrochemical impedance of dielectric elastomers in the physiological environment. Results show that the impedance values among all three investigated elastomers degrade over time. Characteristic time of degradation, ion-concentration-dependent conductivity, and simulation results suggest that ions gradually diffuse from the surrounding physiological solution into the dielectric elastomers. Ionic conductivities of soaked dielectric elastomers can reach 10^{-8} S/m, which is 2−6 orders of magnitude higher than that in pristine elastomers. The effective diffusivity is estimated to be on the order of 10^{-17} m^2/s. Our results demonstrate that the thickness of the dielectric elastomer needs to be thicker than 40 μm to prevent the degradation of the dielectric impedance after 1 year implantation to the value that significantly impacts the bandwidth of the signal transmission in fully stretchable devices. In addition, our results demonstrate that increasing the conductivity and interfacial impedance of the stretchable conductor could reduce the low-frequency losses. Therefore, using dielectric elastomers to passivate nanoscale thick, flexible metal electrodes with high conductivities can be realized with a stable performance in physiological conditions. Whereas this design does not provide stretchability, it can further reduce the total bending stiffness of the device. Regarding fully stretchable devices, the conductivity of the stretchable conductor is required to be higher than 4×10^2 S/m to maintain the performance of the device with geometry and aspect ratio that have been investigated in this study. This work focuses on several commercially available dielectric elastomers, but we also note the ongoing development of novel viscoelastic and self-healing dielectric elastomers. Their applicability in bioelectronics, especially when used for long-term recording and implantation, needs be carefully characterized.

■ ASSOCIATED CONTENT

Supporting Information

The Supporting Information is available free of charge at https://pubs.acs.org/doi/10.1021/acs.nanolett.9b03705.

EIS setup (S1). Chromium/Gold electrodes (S2). Preparation of thin film dielectrics encapsulating electrodes. Cr/Au Electrodes EIS − Bode Plots (S3). Data acquisition. Fitting procedure for Nyquist plots. Schematics of Nyquist plots (S4). Height profiles (S5). Molecular dynamics simulations. Computer-generated PIB plus water structure (S6). Computed densities of PIB and SU-8 at different temperatures (S7). Coating of a stretchable electrode (S8). Resistance of silver-nanoparticles−polymer composite (S9). Stretchable electrodes EIS−Bode Plots (S10). Lossy transmission line bandwidth calculations (PDF)

■ AUTHOR INFORMATION

Corresponding Author

*E-mail: jia_liu@seas.harvard.edu. Phone: 617-496-8119.

ORCID

Paul Le Floch: 0000-0001-7211-1699
Nicola Molinari: 0000-0002-2913-7030
Boris Kozinsky: 0000-0002-0638-539X
Zhigang Suo: 0000-0002-4068-4844
Jia Liu: 0000-0003-2217-6982

Author Contributions

The manuscript was written through contributions of all authors. All authors have given approval to the final version of the manuscript.

Notes

The authors declare no competing financial interest.

■ ACKNOWLEDGMENTS

The authors gratefully acknowledge software support from Schrödinger Inc. in this work and Asahi Kasei for providing the SEBS polymer. We also thank J. C. Salant and D. Kong for their valuable contributions to the production of this manuscript. The work was partially supported by NSF

DOI: 10.1021/acs.nanolett.9b03705
Nano Lett. 2020, 20, 224−233

MRSEC (DMR-14-20570) and the Harvard University Center for Nanoscale Systems supported by the National Science Foundation.

■ ABBREVIATIONS

EIS, Electrochemical Impedance Spectroscopy; PBS, Phosphate Buffered Saline; DI, Deionized; SEBS, Styrene−Ethylene−Butylene−Styrene; PIB, Polyisobutylene; PDMS, Polydimethylsiloxane; EIS, Electrochemical Impedance Spectrum; MD, Molecular Dynamics; MSD, Mean Square Displacement; CNT, Carbon Nanotubes; DAC, Data Acquisition Card

■ REFERENCES

(1) Kim, J.; Ghaffari, R.; Kim, D.-H. The Quest for Miniaturized Soft Bioelectronic Devices. *Nat. Biomed. Eng.* **2017**, *1* (3), 0049.
(2) Lacour, S. P.; Courtine, G.; Guck, J. Materials and Technologies for Soft Implantable Neuroprostheses. *Nat. Rev. Mater.* **2016**, *1* (10), 16063.
(3) Polikov, V. S.; Tresco, P. A.; Reichert, W. M. Response of Brain Tissue to Chronically Implanted Neural Electrodes. *J. Neurosci. Methods* **2005**, *148* (1), 1−18.
(4) Birmingham, K.; Gradinaru, V.; Anikeeva, P.; Grill, W. M.; Pikov, V.; McLaughlin, B.; Pasricha, P.; Weber, D.; Ludwig, K.; Famm, K. Bioelectronic Medicines: a Research Roadmap. *Nat. Rev. Drug Discovery* **2014**, *13* (6), 399−400.
(5) Someya, T.; Bao, Z.; Malliaras, G. G. The Rise of Plastic Bioelectronics. *Nature* **2016**, *540* (7633), 379−385.
(6) Liu, J.; Fu, T. M.; Cheng, Z.; Hong, G.; Zhou, T.; Jin, L.; Duvvuri, M.; Jiang, Z.; Kruskal, P.; Xie, C.; Suo, Z.; Fang, Y.; Lieber, C. M. Syringe-injectable Electronics. *Nat. Nanotechnol.* **2015**, *10* (7), 629−636.
(7) Feiner, R.; Engel, L.; Fleischer, S.; Malki, M.; Gal, I.; Shapira, A.; Shacham-Diamand, Y.; Dvir, T. Engineered Hybrid Cardiac Patches with Multifunctional Electronics for Online Monitoring and Regulation of Tissue Function. *Nat. Mater.* **2016**, *15* (6), 679−85.
(8) Yang, X.; Zhou, T.; Zwang, T. J.; Hong, G.; Zhao, Y.; Viveros, R. D.; Fu, T. M.; Gao, T.; Lieber, C. M. Bioinspired Neuron-like Electronics. *Nat. Mater.* **2019**, *18* (5), 510−517.
(9) Kim, D. H.; Lu, N. S.; Ma, R.; Kim, Y. S.; Kim, R. H.; Wang, S. D.; Wu, J.; Won, S. M.; Tao, H.; Islam, A.; Yu, K. J.; Kim, T. I.; Chowdhury, R.; Ying, M.; Xu, L. Z.; Li, M.; Chung, H. J.; Keum, H.; McCormick, M.; Liu, P.; Zhang, Y. W.; Omenetto, F. G.; Huang, Y. G.; Coleman, T.; Rogers, J. A. Epidermal Electronics. *Science* **2011**, *333* (6044), 838−843.
(10) Tian, B.; Liu, J.; Dvir, T.; Jin, L.; Tsui, J. H.; Qing, Q.; Suo, Z.; Langer, R.; Kohane, D. S.; Lieber, C. M. Macroporous Nanowire Nanoelectronic Scaffolds for Synthetic Tissues. *Nat. Mater.* **2012**, *11* (11), 986−994.
(11) Liu, Y.; Liu, J.; Chen, S.; Lei, T.; Kim, Y.; Niu, S.; Wang, H.; Wang, X.; Foudeh, A. M.; Tok, J. B.; Bao, Z. Soft and Elastic Hydrogel-based Microelectronics for Localized Low-voltage Neuromodulation. *Nat. Biomed. Eng.* **2019**, *3* (1), 58−68.
(12) Kang, J.; Tok, J. B. H.; Bao, Z. Self-healing Soft Electronics. *Nat. Electron.* **2019**, *2* (4), 144−150.
(13) Minev, I. R.; Musienko, P.; Hirsch, A.; Barraud, Q.; Wenger, N.; Moraud, E. M.; Gandar, J.; Capogrosso, M.; Milekovic, T.; Asboth, L.; Torres, R. F.; Vachicouras, N.; Liu, Q.; Pavlova, N.; Duis, S.; Larmagnac, A.; Voros, J.; Micera, S.; Suo, Z.; Courtine, G.; Lacour, S. P. Biomaterials. Electronic Dura Mater for Long-term Multimodal Neural Interfaces. *Science* **2015**, *347* (6218), 159−63.
(14) Trung, T. Q.; Lee, N. E. Recent Progress on Stretchable Electronic Devices with Intrinsically Stretchable Components. *Adv. Mater.* **2017**, *29* (3), 1603167.
(15) Yan, X. Z.; Liu, Z. Y.; Zhang, Q. H.; Lopez, J.; Wang, H.; Wu, H. C.; Niu, S. M.; Yan, H. P.; Wang, S. H.; Lei, T.; Li, J. H.; Qi, D. P.; Huang, P. G.; Huang, J. P.; Zhang, Y.; Wang, Y. Y.; Li, G. L.; Tok, J. B. H.; Chen, X. D.; Bao, Z. A. Quadruple H-Bonding Cross-Linked Supramolecular Polymeric Materials as Substrates for Stretchable, Antitearing, and Self-Healable Thin Film Electrodes. *J. Am. Chem. Soc.* **2018**, *140* (15), 5280−5289.
(16) Song, E. M.; Li, R.; Jin, X.; Du, H. N.; Huang, Y. M.; Zhang, J. Z.; Xia, Y.; Fang, H.; Lee, Y. K.; Yu, K. J.; Chang, J. K.; Mei, Y. F.; Alam, M. A.; Huang, Y. G.; Rogers, J. A. Ultrathin Trilayer Assemblies as Long-Lived Barriers against Water and Ion Penetration in Flexible Bioelectronic Systems. *ACS Nano* **2018**, *12* (10), 10317−10326.
(17) Fang, H.; Zhao, J. N.; Yu, K. J.; Song, E. M.; Farimani, A. B.; Chiang, C. H.; Jin, X.; Xue, Y. G.; Xu, D.; Du, W. B.; Seo, K. J.; Zhong, Y. D.; Yang, Z. J.; Won, S. M.; Fang, G. H.; Choi, S. W.; Chaudhuri, S.; Huang, Y. G.; Alam, M. A.; Viventi, J.; Aluru, N. R.; Rogers, J. A. Ultrathin, Transferred Layers of Thermally Grown Silicon Dioxide as Biofluid Barriers for Biointegrated Flexible Electronic Systems. *Proc. Natl. Acad. Sci. U. S. A.* **2016**, *113* (42), 11682−11687.
(18) Le Floch, P.; Meixuanzi, S.; Tang, J.; Liu, J.; Suo, Z. Stretchable Seal. *ACS Appl. Mater. Interfaces* **2018**, *10* (32), 27333−27343.
(19) Zhang, A.; Lieber, C. M. Nano-bioelectronics. *Chem. Rev.* **2016**, *116* (1), 215−257.
(20) Chipman, R. A. *Theory and Problems of Transmission Lines*; McGraw-Hill Book Company: New York, 1968.
(21) Bard, A. J.; Faulkner, L. R.; Leddy, J.; Zoski, C. G. *Electrochemical Methods: fundamentals and applications*; Wiley: New York, 1980; Vol. 2.
(22) Jacobs, P.; Lorimer, J.; Russer, A.; Wasiucionek, M. Impedance Studies on the System LiClO4—MEEP. *J. Power Sources* **1989**, *26* (3−4), 483−489.
(23) Munichandraiah, N.; Scanlon, L.; Marsh, R.; Kumar, B.; Sircar, A. Ionic Conductivity and Lithium Electrode Stability in Hydrin: LiBF 4 Elastomers. *J. Appl. Electrochem.* **1994**, *24* (10), 1066−1072.
(24) Ratner, M. A.; Shriver, D. F. Ion Transport in Solvent-free Polymers. *Chem. Rev.* **1988**, *88* (1), 109−124.
(25) Yang, L.; McGhie, A.; Farrington, G. Ionic Conductivity in Complexes of Poly (Ethylene Oxide) and $MgCl_2$. *J. Electrochem. Soc.* **1986**, *133* (7), 1380−1385.
(26) Taylor, D.; MacDonald, A. AC Admittance of the Metal/Insulator/Electrolyte Interface. *J. Phys. D: Appl. Phys.* **1987**, *20* (10), 1277.
(27) Klein, R. J.; Zhang, S.; Dou, S.; Jones, B. H.; Colby, R. H.; Runt, J. Modeling electrode polarization in dielectric spectroscopy: Ion Mobility and Mobile Ion Concentration of Single-ion Polymer Electrolytes. *J. Chem. Phys.* **2006**, *124* (14), 144903.
(28) Liu, C.; Liu, Y.; Sokuler, M.; Fell, D.; Keller, S.; Boisen, A.; Butt, H.-J.; Auernhammer, G. K.; Bonaccurso, E. Diffusion of Water into SU-8 Microcantilevers. *Phys. Chem. Chem. Phys.* **2010**, *12* (35), 10577−10583.
(29) Watson, J.; Baron, M. The Behaviour of Water in Poly (dimethylsiloxane). *J. Membr. Sci.* **1996**, *110* (1), 47−57.
(30) Crank, J. *The Mathematics of Diffusion*; Oxford University Press, 1979.
(31) Kong, D.; Pfattner, R.; Chortos, A.; Lu, C.; Hinckley, A. C.; Wang, C.; Lee, W.-Y.; Chung, J. W.; Bao, Z. Capacitance Characterization of Elastomeric Dielectrics for Applications in Intrinsically Stretchable Thin Film Transistors. *Adv. Funct. Mater.* **2016**, *26* (26), 4680−4686.
(32) Kim, Y. H.; Sachse, C.; Machala, M. L.; May, C.; Müller-Meskamp, L.; Leo, K. Highly Conductive PEDOT:PSS Electrode with Optimized Solvent and Thermal Post-Treatment for ITO-Free Organic Solar Cells. *Adv. Funct. Mater.* **2011**, *21* (6), 1076−1081.
(33) Kim, Y.; Zhu, J.; Yeom, B.; Di Prima, M.; Su, X.; Kim, J. G.; Yoo, S. J.; Uher, C.; Kotov, N. A. Stretchable Nanoparticle Conductors with Self-organized Conductive Pathways. *Nature* **2013**, *500* (7460), 59−63.
(34) Yao, S.; Zhu, Y. Nanomaterial-enabled Stretchable Conductors: Strategies, Materials and Devices. *Adv. Mater.* **2015**, *27* (9), 1480−511.
(35) Matsuhisa, N.; Inoue, D.; Zalar, P.; Jin, H.; Matsuba, Y.; Itoh, A.; Yokota, T.; Hashizume, D.; Someya, T. Printable Elastic

DOI: 10.1021/acs.nanolett.9b03705
Nano Lett. 2020, 20, 224−233

Conductors by in situ Formation of Silver Nanoparticles from Silver Flakes. *Nat. Mater.* **2017**, *16* (8), 834−840.
(36) Yang, M.; Hood, Z. D.; Yang, X.; Chi, M.; Xia, Y. Facile Synthesis of Ag:@Au Core-sheath Nanowires with Greatly Improved Stability against Oxidation. *Chem. Commun.* **2017**, *53* (12), 1965−1968.
(37) Yang, C. H.; Chen, B.; Lu, J. J.; Yang, J. H.; Zhou, J.; Chen, Y. M.; Suo, Z. Ionic Cable. *Extreme. Mechs. Lett.* **2015**, *3*, 59−65.
(38) Choi, S.; Han, S. I.; Jung, D.; Hwang, H. J.; Lim, C.; Bae, S.; Park, O. K.; Tschabrunn, C. M.; Lee, M.; Bae, S. Y.; Yu, J. W.; Ryu, J. H.; Lee, S. W.; Park, K.; Kang, P. M.; Lee, W. B.; Nezafat, R.; Hyeon, T.; Kim, D. H. Highly Conductive, Stretchable and Biocompatible Ag-Au Core-sheath Nanowire Composite for Wearable and Implantable Bioelectronics. *Nat. Nanotechnol.* **2018**, *13* (11), 1048−1056.
(39) Jin, L.; Chortos, A.; Lian, F.; Pop, E.; Linder, C.; Bao, Z.; Cai, W. Microstructural Origin of Resistance-strain Hysteresis in Carbon Nanotube Thin Film Conductors. *Proc. Natl. Acad. Sci. U. S. A.* **2018**, *115* (9), 1986−1991.
(40) Carter, W.; Magat, M.; Schneider, W.; Smyth, C. Dielectric Dispersion and Absorption in Natural Rubber, Neoprene, Butaprene NM and Butaprene S, Gum, and Tread Stocks. *Trans. Faraday Soc.* **1946**, *42*, A213−A220.

DOI: 10.1021/acs.nanolett.9b03705
Nano Lett. 2020, 20, 224−233